UC San Diego
International Symposium on Stratified Flows

Title

Boussinesq dynamics of an idealized tropopause

Permalink

https://escholarship.org/uc/item/5h66n59t

Journal

International Symposium on Stratified Flows, 8(1)

Authors

Asselin, Olivier
Bartello, Peter
Straub, David

Publication Date

2016-08-29

Boussinesq dynamics of an idealized tropopause

Olivier Asselin, Peter Bartello and David Straub

McGill University
olivier.asselin@mail.mcgill.ca

Abstract

The near-tropopause flow has been interpreted using quasigeostrophic (QG) theory. Asselin et al. (2016) showed that this simplified dynamical framework is inconsistent. In the vicinity of rapid changes in stratification such as those characterizing the tropopause, QG flows develop statically unstable conditions. In this paper, a simple yet self-consistent Boussinesq model of the near-tropopause flow is proposed. As expected, the Boussinesq model reduces to the QG model in the limit where the Rossby number is much smaller than ϵ, the nondimensional height scale characterizing the stratification change. In the more relevant case where the Rossby number is larger than ϵ but still smaller than unity, analysis and numerical simulations suggest that Boussinesq dynamics inhibit the development of statically unstable density profiles. Additionally, tropopause displacements are to found to scale with the Rossby number.

1   Introduction

The quasigeostrophic (QG) approximation has been used extensively to model tropospheric dynamics at mid-latitudes. Under such balanced conditions, the potential vorticity distribution can be inverted to deduce all the other dynamical variables (eg. Hoskins et al. (1985)). Tropopause motion plays a crucial role in the dynamics, because potential vorticity anomalies are generally strongest there. Blumen (1978) considered a simplified configuration whereby the tropopause is treated as a rigid lid overlying a semi-infinite domain with uniform potential vorticity. In this surface quasigeostrophic (SQG) model, the flow is everywhere determined by the distribution of temperature anomalies at the tropopause. Tulloch and Smith (2006) showed that the finite-depth version of Blumen's model produces an energy spectrum similar to that observed near the tropopause (eg. Nastrom and Gage (1985)). The SQG model can also be derived as a limit of QG in which the stratification profile undergoes a discontinuous jump (eg. Juckes (1994), Held et al. (1995)). The rigid-lid approximation is thus not formally required and the stratospheric flow may be taken into account. More recently, Plougonven and Vanneste (2010) and Smith and Bernard (2013) examined the more realistic case of a rapid yet continuous transition in the stratification profile.

Asselin et al. (2016) showed that only very weak QG flows are self-consistent near the tropopause. In the presence of a sharp transition in the stratification profile, QG dynamics produce comparably sharp vertical gradients of perturbation buoyancy. These small vertical scales imply locally large Froude numbers. For realistic atmospheric parameters, not only does QG break down, but statically unstable conditions also develop. In this contribution we describe a simple yet self-consistent Boussinesq model of the near-tropopause flow. In the next section, we analyze near-tropopause Boussinesq dynamics in the limit of low Rossby number and compare them to the QG case. Leading order dynamics suggest that Boussinesq flows have a lessened tendency to static instability and tropopause displacements scale with the Rossby number. In Section 3, we use numerical simulations to confirm our analysis. Section 4 briefly discusses the results.

2 Analysis

2.1 QG dynamics

The development of statically unstable conditions can be understood by examining the evolution equation for b_z, the vertical derivative of perturbation buoyancy. Under quasi-geostrophic dynamics this equation takes the form:

$$\frac{Db_z}{Dt} = -w_z N^2 - w N_z^2, \qquad \text{(QG)} \tag{1}$$

where $D/Dt = \partial/\partial t + \mathbf{u}\cdot\nabla$ is the horizontal material derivative, $\mathbf{u}$ and w are the horizontal and vertical velocities, $N^2 = N^2(z)$ is the base-state stratification profile and where the symbol N_z^2 is taken to mean $d(N^2)/dz$. Following Smith and Bernard (2013), we assume a hyperbolic tangent N profile that varies over a small vertical scale, h, characterizing the tropopause height scale. Asselin et al. (2016) showed analytically and numerically that the vertical velocity remains vertically smooth near the tropopause — $w_z \sim w/H$, where H is a characteristic (smooth) vertical scale. In the vicinity of the tropopause, the ratio of the first over the second term on right-hand side of (1) scales like $\epsilon \equiv h/H$. The leading order dynamics thus reduce to

$$\frac{Db_z}{Dt} \approx -w N_z^2. \qquad \text{(Near-tropopause, QG)} \tag{2}$$

Strong intensification of b_z features occurs through the $w N_z^2$ term, and thus may only take place in the transition region, defined as $z < |h|$. This is consistent with our earlier work, which interpreted the development of statically unstable conditions from the point of view of a differential advection of buoyancy above and below the stratification jump. In the transition region, buoyancy develops h-scale features — strong b_z patches — and thus unstable density profiles unless the flow is very weak.

2.2 Boussinesq dynamics

In contrast with QG, Boussinesq dynamics retain the effects of the vertical advection of perturbation buoyancy. The evolution equation for b_z may be written as

$$\frac{Db_z}{Dt} + (\mathbf{u}_z \cdot \nabla)b = -w_z(N^2 + b_z) - w(N^2 + b_z)_z. \qquad \text{(BO)} \tag{3}$$

We now perform a scale analysis in order to obtain a simplified picture of near-tropopause Boussinesq dynamics in the case where the Rossby and Froude numbers are comparably small. More precisely, we study the case $Ro \sim Fr \sim \epsilon$, where $Ro = U/fL$ is the Rossby number, $Fr = U/NH$ is the Froude number, f is the coriolis parameter, U and L are the characteristic velocity and horizontal length scales and $\epsilon \equiv h/H$ is the nondimensional height scale characterizing the stratification jump. We further assume[1] that the velocity field varies smoothly in the vertical — $\mathbf{u}_z \sim \mathbf{u}/H$, $w_z \sim w/H$ — but that buoyancy may vary on the scale of the stratification jump — $b_z \sim b/h$. At leading order, the b_z equation then reduces to

$$\frac{Db_z}{Dt} \approx -w N_z^2 + w b_{zz}. \qquad \text{(Near-tropopause, BO)} \tag{4}$$

---

[1]This was confirmed by numerical simulations (not shown here).

It is instructive to compare this equation with (2), its QG counterpart. At leading order, the equations mainly differ by the presence of vertical advection. Importantly, this term does not partake in the growth of b_z structures. To make this explicit, one may write the above equation in terms of a total, three-dimensional material derivative,

$$\frac{db_z}{dt} \approx -wN_z^2. \qquad \text{(Near-tropopause, BO)} \qquad (5)$$

For both the QG and Boussinesq cases, it is only through the wN_z^2 term that b_z may strongly grow. That is, large b_z patches may only be generated in the transition region, $|z| < h$. In the QG case, there is no vertical advection and patches are trapped in this region. In the Boussinesq case, however, the patches are advected away from the transition region — the only place they can experience significant growth. As such, we expect Boussinesq dynamics to lessen the tendency to static instability. Let us now consider the argument more quantitatively.

Leading order dynamics suggest that the growth of b_z occurs over a characteristic time scale, $\tau_1 = L/U$. That is, one expects vertical velocity to switch signs over τ_1 on average. In Boussinesq dynamics, however, vertical advection may push the b_z patches out of the transition region. In such case, growth stops when the patches leave this region, $i.e.$ after a characteristic residence time, $\tau_2 = h/W$. Assuming standard QG scaling for the vertical velocity, $W \sim RoUH/L$, the timescales are related by:

$$\tau_2 = \left(\frac{\epsilon}{Ro}\right)\tau_1. \qquad (6)$$

We now perform a scale analysis on the b_z evolution equation, (5). Assuming b_z to be initially small, we obtain a quantitative measure of stability at the end of the growth period, $\tau \equiv \min(\tau_1, \tau_2)$:

$$\frac{|b_z|}{N^2} \sim \frac{W\tau}{h} = \begin{cases} Ro/\epsilon & \text{if } Ro < \epsilon, \\ 1 & \text{if } Ro > \epsilon. \end{cases} \qquad (7)$$

Similarly, the expected characteristic vertical scale of buoyancy, γ, may be estimated as

$$\gamma \sim \left|\frac{b}{b_z}\right| \sim \frac{h\tau_1}{\tau} = \begin{cases} h & \text{if } Ro < \epsilon, \\ h(Ro/\epsilon) & \text{if } Ro > \epsilon. \end{cases} \qquad (8)$$

If $Ro < \epsilon$, the growth time is given by τ_1. That is, vertical advection is too weak to push b_z patches away from the intensification region. As in the QG case, bouyancy develops h-scale features, but the flow is so weak that it remains statically stable. Interestingly, the QG approximation is strictly valid only if $Ro \ll \epsilon$. This is consistent with our earlier work. In the more relevant limit where $Ro > \epsilon$, however, vertical advection is strong enough to push the b_z patches away from the transition region. Growth thus ceases after a characteristic time τ_2. Interestingly, scale analysis suggests that negative patches leave the intensification region with marginal stability. By contrast, a similarly strong QG flow would satisfy the necessary condition for static instability. Therefore, Boussinesq dynamics inhibit the development of statically unstable density profiles in the range $\epsilon < Ro \ll 1$.

Table 1: Key parameters of the numerical simulations.

Domain size (km³)	$15000 \times 15000 \times 20$
Frequencies (s⁻¹)	$N_t = 0.01, \quad N_s = 0.02, \quad N_0 = (N_t + N_s)/2, \quad f = 0.0001$
Resolution	$N_x = N_y = N_z = 256$
Initial energy peak	$k_H^i = 5, \quad k_z^i = 1$
Grid spacing	$\Delta x = \Delta y = (N_0 k_H^i / f k_z^i)\Delta z, \quad h = 2\Delta z$

2.3 Tropopause displacement

The above analysis also sheds light on the tropopause displacement, η, which we define as the height at which the total stratification reaches the average value of the base state:

$$N^2(\eta) + b_z(x, y, \eta, t) \equiv N_0^2, \tag{9}$$

where $N_0 = N(0)$. Perturbation buoyancy depends on all space and time variables, and thus η is a two-dimensional surface that evolves with time. In Earth's atmosphere, the change in N^2 across the tropopause is comparable to N^2 itself (see Table 1). As such, significant tropopause displacements are expected when $b_z \sim N^2$. According to the above analysis, b_z structures grow to comparable magnitudes when $\epsilon < Ro \ll 1$. One thus expects the tropopause displacement to approximately match the location of these structures. On average, vertical advection will push these structures over a characteristic distance

$$|\eta| \sim \tau_1 W = RoH. \qquad (\epsilon < Ro \ll 1) \tag{10}$$

Therefore, in this low-Ro range, we expect the amplitude of the tropopause displacement to grow with the Rossby number. This is consistent with earlier works by Rivest et al. (1992) and Juckes (1994). In the limit of very weak flow, $Ro < \epsilon$, no significant tropopause displacement is expected.

3   Numerical simulations

In order to test the above analysis, we conduct numerical integrations of the Boussinesq equations for various flow strengths, U, and compare them with a QG control run. Following Asselin et al. (2016), the model is initialized with smooth geostrophically balanced initial conditions superimposed on a rapidly-varying background stratification profile. The Rossby and Froude numbers are based on the horizontal and vertical length scales at which energy is initially located. Initial conditions and parameters, outlined in Table 1, are set so that $Ro = Fr$ for all simulations. The flow is freely decaying under the influence of hyperviscosity. Vertical diffusion is absent in order to facilitate comparison with the QG version of the model. For more detail on the model the reader is referred to Asselin et al. (2016).

Figure 1 shows the early time evolution of b_z and the associated tropopause displacement. As anticipated from leading order dynamics, (5), strong patches are concentrated near the transition region. Also, intensifying positive (negative) patches sink (rise). This translates
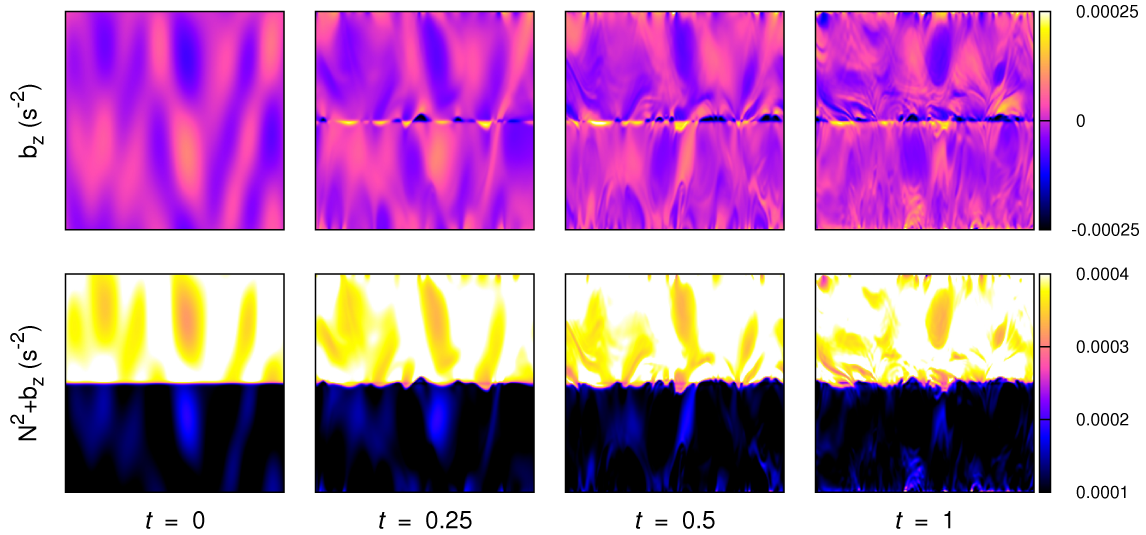
Figure 1: Snapshots of b_z (upper panels) and total buoyancy frequency $N^2 + b_z$ (lower panels) on the xz plane during the first turnover time in the Boussinesq simulation with $Ro = 0.03$ (or $U = 3$ m/s).

into tropopause undulations. The above analysis predicted that the amplitude of these undulations grows linearly with the Rossby number. This is confirmed in the left panel of Figure 2, which depicts the time-averaged tropopause displacement over a range of Rossby numbers. For stronger flows, the dependency on Ro is no longer linear. Unstable patches away from the near-tropopause region are then more frequent and our definition of the tropopause, (9), becomes less meaningful. The right panel of Figure 2 shows the time-averaged vertical scale of buoyancy, γ, in the transition region. At very low Ro, both the Boussinesq and QG simulations produce h-scale buoyancy features. That is, γ/h is near unity. At higher Ro, Boussinesq dynamics produce smoother vertical scales. As expected from our scale analysis, there is a significant range of Ro for which γ increases linearly with Ro.
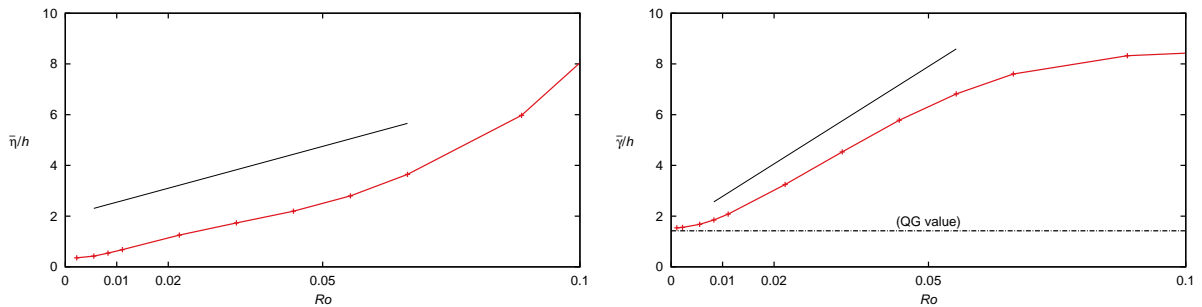

Figure 2: Time-averaged root mean square tropopause displacement η (left panel) and vertical scale of buoyancy γ (right panel) in the transition region. Both quantities are normalized by the transition region height scale, h. The solid guidelines suggest a linear dependency upon Ro.

Figure 3 shows the growth rate of static instability as a function of time and the Rossby number. More precisely, we average real values of $\sigma = \sqrt{-(N^2 + b_z)}/N_0$ over an extended transition region, $|z| < 10h$. As such, tropopause undulations are generally included in the averaging domain ($\bar{\eta} < 10h$ in the left panel of Figure 2). Note also that the growth rate is set to zero if $N^2 + b_z \geq 0$. It is clear from this figure that Boussinesq simulations have a lessened tendency to static instability. In the QG simulation, the growth rate

quickly increases as differential advection of buoyancy produces h-scale features. By contrast, the lower Ro Boussinesq simulations have vanishingly small growth rates. This is consistent with the prediction that b_z structures leave the intensification region with marginal stability. In the higher Ro cases, the flow has significant regions of instability from the onset of the simulation. Therefore, one cannot assume that $Ro \ll 1$, and the analysis of Section 2 does not hold. Correspondingly, neither η nor γ linearly depends on Ro in this range. The right panel displays the time-averaged growth rate as a function of the Rossby number. Interestingly, the Boussinesq flow needs to be roughly 10 times stronger than the QG flow to be as unstable.
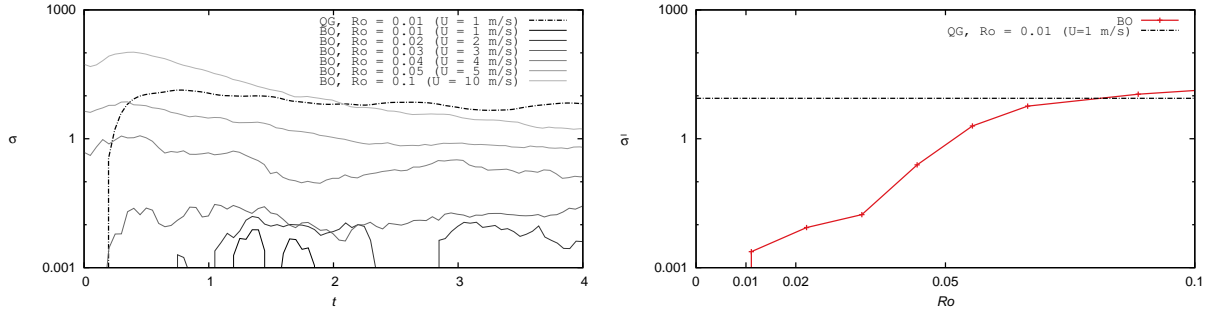

Figure 3: Left-panel: Time evolution of the static instability growth rate for various Ro. Right panel: Time-averaged (between $t = 1$ and $t = 2$) growth rate as a function of Ro. The QG simulation (with effective $Ro = 0.01$) is represented with dashed lines. The growth rate is normalized by N_0 and averaged over an extended transition region $|z| < 10h$.

4 Discussion

In this paper, we have described a simplified picture of the near-tropopause flow based on Boussinesq dynamics. From this point of view, statically unstable conditions develop because perturbation buoyancy feeds on the base-state buoyancy in the transition region. This interpretation provides us with interesting insights on low-Ro Boussinesq dynamics and facilitates comparison with the QG case. However, this separation into perturbation and base-state components is arbitrary in Boussinesq or more general models: only the total stratification is dynamically relevant. Future work will adopt this point of view, whereby the total stratification is advected by a three-dimensional velocity field. The present analysis assumed that the Rossby and Froude numbers were comparable to the small nondimensional tropopause width, ϵ. Future work will also consider more realistic regimes. For instance, the near-tropopause flow would be better characterized by stronger winds, say $U \sim 10$ m/s.

References

Asselin, O., Bartello, P., and Straub, D. N. (2016). On quasigeostrophic dynamics near the tropopause. *Physics of Fluids (1994-present)*, 28(2):026601.

Blumen, W. (1978). Uniform potential vorticity flow: Part i. theory of wave interactions and two-dimensional turbulence. *Journal of the Atmospheric Sciences*, 35(5):774–783.

Held, I. M., Pierrehumbert, R. T., Garner, S. T., and Swanson, K. L. (1995). Surface quasi-geostrophic dynamics. *Journal of Fluid Mechanics*, 282:1–20.

Hoskins, B. J., McIntyre, M., and Robertson, A. W. (1985). On the use and significance of isentropic potential vorticity maps. *Quarterly Journal of the Royal Meteorological Society*, 111(470):877–946.

Juckes, M. (1994). Quasigeostrophic dynamics of the tropopause. *Journal of the Atmospheric Sciences*, 51(19):2756–2768.

Nastrom, G. and Gage, K. S. (1985). A climatology of atmospheric wavenumber spectra of wind and temperature observed by commercial aircraft. *Journal of the atmospheric sciences*, 42(9):950–960.

Plougonven, R. and Vanneste, J. (2010). Quasigeostrophic dynamics of a finite-thickness tropopause. *Journal of the Atmospheric Sciences*, 67(10):3149–3163.

Rivest, C., Davis, C. A., and Farrell, B. F. (1992). Upper-tropospheric synoptic-scale waves. part i: Maintenance as eady normal modes. *Journal of the atmospheric sciences*, 49(22):2108–2119.

Smith, K. S. and Bernard, E. (2013). Geostrophic turbulence near rapid changes in stratification. *Physics of Fluids (1994-present)*, 25(4):046601.

Tulloch, R. and Smith, K. (2006). A theory for the atmospheric energy spectrum: Depth-limited temperature anomalies at the tropopause. *Proceedings of the National Academy of Sciences*, 103(40):14690–14694.